

Learning Adaptive Multi-Objective Robot Navigation Incorporating Demonstrations

Jorge de Heuvel

Tharun Sethuraman

Maren Bennewitz

Abstract—Preference-aligned robot navigation in human environments is typically achieved through learning-based approaches, utilizing user feedback or demonstrations for personalization. However, personal preferences are subject to change and might even be context-dependent. Yet traditional reinforcement learning (RL) approaches with static reward functions often fall short in adapting to these varying user preferences, inevitably reflecting demonstrations once training is completed. This paper introduces a framework that combines multi-objective reinforcement learning (MORL) with demonstration-based learning. Our approach allows for dynamic adaptation to changing user preferences without retraining. It fluently modulates between reward-defined preference objectives and the amount of demonstration data reflection. Through rigorous evaluations, including a sim-to-real transfer on two robots, we demonstrate our framework’s capability to reflect user preferences accurately while achieving high navigational performance in terms of collision avoidance and goal pursuance.

I. INTRODUCTION

Recent remarkable advancements in the field of robotics, especially in autonomous mobile robot navigation, have been driven by deep reinforcement learning (RL), enabling end-to-end and nuanced navigation policies. In human environments, optimal human-robot interaction hinges on the alignment AI systems with user preferences and values [1], [2].

Despite progress, traditional RL-based robot navigation has mainly optimized fixed objectives like path efficiency or obstacle avoidance, failing to address the complexities of human-aware navigation, which requires balancing multiple, often conflicting, objectives. Specifically, adherence to proxemic user preferences, approaching behavior, and navigational efficiency [3] are key factors. Furthermore, existing research on navigation often treats user preferences as static [4], and the pre-configured reward functions of traditional RL policies cannot be adapted to changing preferences without retraining, highlighting a significant gap in the current methodology.

To preference-align RL-based navigation around the human, De Heuvel *et al.* [2], [5] have employed an additional behavior cloning loss fed with demonstration data. Yet, the application of preference-aligned navigation strategies raises questions regarding the balance of demonstration-based preferences with respect to baseline objectives and

All authors are with the Humanoid Robots Lab, University of Bonn, Germany. M. Bennewitz and J. de Heuvel are additionally with the Lamarr Institute for Machine Learning and Artificial Intelligence and the Center for Robotics, Bonn, Germany. This work has been partially funded by the BMBF, grant No. 16KIS1949 and within the Robotics Institute Germany, grant No. 16ME0999, as well as by the DFG, grant No. BE 4420/2-2 (FOR 2535 Anticipating Human Behavior).

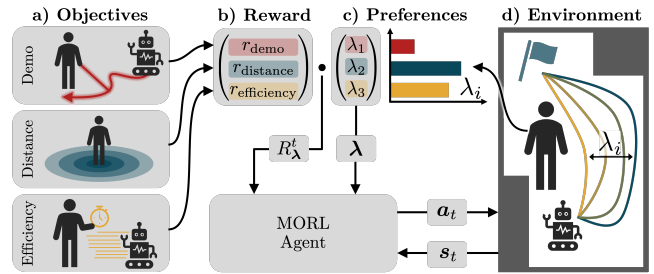


Fig. 1: Our multi-objective reinforcement learning (MORL) navigation agent learns to adapt its behavior to varying preferences captured through reward components and demonstrations without re-training. **a)** The navigation style can fluently shift between demonstration-induced, distance keeping, and efficiency objectives. **b)** We modulate the MORL reward vector r_t with a **c)** varying preference λ , while providing λ as input to the agent. **d)** The resulting human-centered policy can generate a spectrum of trajectories, here sketched for the objectives efficiency and distance-keeping.

contextual adaptability. It becomes essential to devise mechanisms that can modulate the influence of demonstrations and preferences [6].

As a solution, multi-objective reinforcement learning (MORL) emerges [7], enabling instant post-training adaptation of behavior to accommodate changing preferences without the need for retraining. This offers on-the-fly adaptation of various preferences, but also ensures the maintenance of navigational baseline objectives, such as goal pursuance and collision avoidance.

This paper introduces a novel framework combining the flexibility of multi-objective reinforcement learning with the preference-alignment capabilities of demonstration-based learning to address challenges of user-aware robot navigation (see Fig. 1). Navigation behavior can adjust on-the-fly to user preferences without retraining, while meeting basal navigational goal and collision-avoidance objectives. Extensive evaluation demonstrates performance and preference-reflection among both a static and dynamic human. The study concludes with a sim-to-real transfer for an evaluation on two different robots.

In summary, the main contributions of our work are:

- A multi-objective reinforcement learning human-aware robot navigation framework that enables policy adaption to preferences post training.
- The incorporation of demonstration data as a tuneable objective.
- A smooth real-world transfer and evaluation on two different robots.

II. RELATED WORK

The concept of personalized navigation is gaining traction, focusing on robots adapting strategies based on individual

preferences. Users can express preferences through ranking trajectory queries [8], [9] or providing demonstrations [2], [5]. Both feedback types can distill a preference-aligned navigation policy. This work establishes a demonstration-infused policy that aligns on-the-fly without retraining, by combining multi-objective reinforcement learning (MORL) and demonstration data.

MORL enhances traditional RL by optimizing multiple objectives simultaneously. Traditional navigation approaches have long leveraged multi-objective formulations [10], [11], [12]. While MORL frameworks exist for discrete [13] and continuous action spaces [14], [15], unified benchmarking libraries [16] are still emerging. Nonetheless, MORL has been applied to autonomous driving [17], and robotic tasks like manipulation [18] and navigation [6], [19].

In mobile robot navigation, Marta *et al.* [6] demonstrate interpolation between human feedback-derived navigational preferences and baseline objectives using a social force model guiding the robot among pedestrians. While their model uses pairwise trajectory queries, we adjust the influence of demonstration data on a policy directly driving the robot.

Ballou *et al.* [20] used meta reinforcement learning to adjust robot navigation among humans, efficiently fine-tuning policies for changes in the reward function, such goal pursuance or distance keeping. However, their adaptation to shifting objectives is not instantaneous, but requires and adaption training phase. In contrast, our MORL policy adapts to preference weight changes immediately, without retraining.

The closest to our study is Choi *et al.* [8], who use multi-agent training with parameterized rewards [21] for adaptable navigation. Agents start with random reward weights each episode, and preferences are estimated via Bayesian inference in a human feedback loop. In contrast to their objective parameterization, our MORL agent separately estimates Q -values for the different objectives.

Lee *et al.* [21] presented an approach, where a high-level skill agent adjusts the behavior of a low-level tunable navigation agent using a parameterized reward function. This two-step training process separates high- and low-level agent training. The high-level agent's optimized skill vector provides insights into context-dependent reward priorities.

III. OUR APPROACH

A. Problem Statement

We consider a wheeled robot navigating in the vicinity of a human and unknown obstacles, pursuing a local goal while avoiding collisions. The human has certain preferences about the navigation style of the robot that may change depending on navigational context. These navigation preferences can be expressed in the form of demonstrations, e.g., through a VR interface [2]. We assume the robot can reliably estimate the its own and human position in the environment, obstacles are perceived by the robot through 2D lidar. The navigation policy processes sensor and goal information along with a preference vector containing user

preferences to generate style-adapted navigation behavior through velocity commands.

B. Multi-Objective Reinforcement Learning

Multi-objective reinforcement learning (MORL) enhances traditional RL by integrating multiple, often conflicting, objectives [7]. In MORL, the agent is trained to learn policies that strike a balance among these diverse objectives, as opposed to a singular reward function.

The MORL problem is formulated within the framework of a Markov Decision Process (MDP), defined by the tuple $(\mathcal{S}, \mathcal{A}, \mathcal{P}, \mathcal{R}, \gamma)$. Here, \mathcal{S} is the state space, \mathcal{A} is the action space, $\mathcal{P} : \mathcal{S} \times \mathcal{A} \times \mathcal{S} \rightarrow [0, 1]$ is the state transition probability, and γ is the discount factor. A distinctive feature of MORL is the multi-dimensional reward function $\mathcal{R} : \mathcal{S} \times \mathcal{A} \rightarrow \mathbb{R}^n$, which outputs a vector of rewards \mathbf{r}_t for n different objectives.

A single policy optimally adheres to a given set of preferences, represented by the convex preference weight vector $\lambda \in \mathbb{R}^n$. The policy $\pi_\lambda(s)$ optimizes a scalarized reward function $R_\lambda(s, a) = \lambda^\top \mathbf{r}(s, a)$, itemizing the different objectives.

We employ the MORL-TD3 implementation of Basaklar *et al.* [14], which introduces four major modifications to TD3's standard actor-critic-structure with respect to the policy loss and preference-space exploration for improved training efficiency, robustness, and preference-reflection: Firstly, a preference interpolator $I(\lambda) = \lambda_p$ projects the original preference vectors λ into a normalized solution space, thereby aligning preferences with multi-objective value solutions Q . Secondly, the framework is complemented by angle loss $g(\lambda_p, Q)$, designed to minimize the directional angle between the interpolated preference vectors λ_p and the multi-objective vector Q . The actor network is updated by maximizing the term $\lambda^\top Q$, where λ is the original convex preference vector and Q is the critic network's output, while simultaneously minimizing the directional angle term. Thirdly, to efficiently learn across the entire preference space in MORL-TD3, a hindsight experience replay mechanism [22] enhances the preference vector diversity during training, enabling the policy to adapt to various objectives more effectively. Fourthly, the training process involves running a number of C_p environments in parallel for N time steps, each tailored to explore a distinct segment of the preference vector space.

1) *State and Action Space*: The state space includes the local goal, human position, and obstacles detected by a lidar sensor. The agent receives the relative 2D goal location \mathbf{p}_g and human position \mathbf{p}_h in polar coordinates. The 360° lidar scan, with a range of 4m, is min-pooled from 720 to $N_{\text{lidar}} = 30$ rays. These are combined in the state vector as $s_t = (\mathbf{p}_g, \mathbf{p}_h, \mathcal{L}_t)$, where $\mathcal{L}_t = d_i^t | 0 \leq i < N_{\text{lidar}}$.

The robot is controlled at 5Hz with linear and angular velocity commands $a_t = (v, \omega)$, where $v \in [0, 0.5] \text{ m s}^{-1}$ and $\omega \in [-\pi, \pi] \text{ rad s}^{-1}$.

2) *Networks*: The networks of actor, critic, behavior cloning policy, and reward model (see below) are fully-

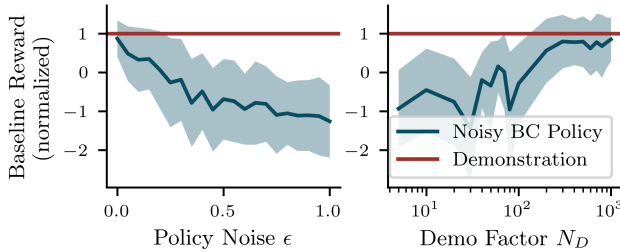


Fig. 2: Exploration of D-REX-related demonstration parameters averages over 20 trajectory rollouts, measured against the optimal demonstration behavior's reward. **a)** The execution of the ϵ -greedy noise-injected behavior cloning (BC) policy trained with a demonstration augmentation factor of $N_D = 1,000$ reveals a degradation of navigation performance measured by the normalized baseline reward with growing strength of the injected noise. **b)** The demonstration augmentation factor N_D indicates how many times the human-centric oracle demonstration trajectory (see Sec.III-D.3) was rolled out with randomized obstacle placement to form the training dataset, showing increased performance with higher N_D .

connected multi-layer perceptron (MLP) networks that share the same architecture of 4 layers with 256 neurons each.

C. Incorporating Demonstrations

As one of our our main contributions, we distill nuanced preferences from demonstration trajectories τ into a reward model that natively integrates into MORL as one of the objectives and guides the learning agent to demonstration-like behavior, directly modulated by λ . Through this novel design choice, the influence of demonstrations can be modulated post-training.

In a typical RL from human feedback setting [6], a reward model is derived from pairwise A \succ B preference queries in a human feedback process via a ranking loss. However, demonstrations provided are typically considered equally important, rendering unsuitable for a reward model. To address the problem of non-existent ranking from demonstration data, we employ the disturbance-based reward extrapolation (D-REX) approach by Brown *et al.* [23], which imitates pairwise A \succ B preference queries by ranking over noise-injected demonstration trajectories. First, a behavior cloning (BC) policy π_{BC} is trained from N_D demonstration trajectories. Subsequently, the BC policy $\pi_{BC}(\cdot|\epsilon)$ is executed with increasing level of ϵ -greedy policy noise $\epsilon \in \mathcal{E} = (\epsilon_1, \epsilon_2, \dots, \epsilon_d)$ with $\epsilon_1 > \epsilon_2 > \dots > \epsilon_d$. In short, low-noise trajectories almost perfectly resemble the demonstration trajectory, while they slowly loose their shape with growing levels of noise. Trajectory rollouts generated with lower noise are automatically ranked superior compared to their higher-noise counterparts. Finally, a rich preference-ranking dataset

$$D_{\text{rank}} = \{\tau_i \prec \tau_j \mid \tau_i \sim \pi_{BC}(\cdot|\epsilon_i), \tau_j \sim \pi_{BC}(\cdot|\epsilon_j), \epsilon_i > \epsilon_j\}$$

is obtained. From D_{rank} , we train a reward model $\hat{R}(s, a) \in [0, 1]$ using the Bradley-Terry model [24] implemented as a binary cross entropy loss such that $\sum_{s \in \tau_i} \hat{R}_\theta(s, a) < \sum_{s \in \tau_j} \hat{R}_\theta(s, a)$ when $\tau_i \prec \tau_j$.

For our ranking dataset D_{rank} , we choose a noise range $\mathcal{E} = (0, \dots, 0.2)$ and obtain $N_D = 1,000$ demonstration augmentations from a single human-centric demonstration trajectory pattern in a obstacle-randomized environment compare Fig. 2 and Sec. III-D.3.

D. Reward

The reward function covers traditional navigational baseline objectives, and three tuneable distinct style objectives based on quantifiable metrics and preference demonstrations. In our MORL setup, the baseline objectives are summed and occupy the first entry in the reward vector \mathbf{r}_t which is assigned a static preference weight of one. Note that this is neglected in further notations of the convex vector λ to focus on the tuneable objectives. For the other objectives occupying entries in the reward vector, the preference weights are dynamic.

The reward vector for our MORL framework consists of

$$\mathbf{r}_t = (\underbrace{r_{\text{baseline}}^t, r_{\text{distance}}^t, r_{\text{efficiency}}^t}_{\text{static}}, \underbrace{r_{\text{demo}}^t}_{\text{dynamic objectives}}), \quad (1)$$

as explained below.

1) *Baseline*: The agent must exhibit goal pursuance and collision avoidance. Goal-oriented navigation uses a continuous reward $r_{\text{goal}}^t = 125 \cdot (d_g^t - d_g^{t-1})$, based on the change in distance $d_g = |\mathbf{p}_g|$ from the goal. The total cumulative goal reward $R = \sum_{t=0}^T r_{\text{goal}}^t$ is non-discounted to remain independent of the number of steps to the goal, avoiding a bias towards shortest paths and thus the efficiency preference objective. Collision avoidance uses a sparse penalty $r_{\text{collision}}^t = -1,000$ for contact between the robot and any obstacle. The baseline reward function is $r_{\text{baseline}}^t = r_{\text{goal}}^t + r_{\text{collision}}^t$.

2) *Tuneable Style Objectives*: Our three style objectives cover proxemics, efficiency, and demonstration-reflection: To include proxemics, an important comfort factor in human-aware navigation, we define a quadratic distance penalty for positional closeness $d_h = |\mathbf{p}_h|$ to the human within a range $d_{\text{thresh}} = 2\text{m}$ as

$$r_{\text{distance}}^t = -10 \frac{(d_h - d_{\text{thresh}})^2}{(d_{\text{thresh}} - d_{\min})^2} \text{ if } d_h \leq d_{\text{thresh}}, \quad (2)$$

else zero, with $d_{\min} = 0.3\text{m}$.

The second style objective is navigational efficiency, or shortest path navigation, implemented with a constant time penalty $r_{\text{efficiency}}^t = -10$.

The third and last objective is demonstration-like behavior r_{demo}^t , as elaborated below. Note that all rewards of the tuneable objectives are defined as penalties with identical ranges of $[-10, 0]$.

3) *Demonstration Acquisition and Reward*: Demonstrations may capture nuanced navigation styles which are difficult to express using an analytical reward function, such as characteristically-shaped trajectories when approaching the user. In this work, we rely on a demonstration oracle that generates an optimal demonstration pattern, see Fig. 3, where the robot circumnavigates the human in a distinct circular manner. After directly approaching the human, at $d_h = 1\text{m}$ it executes a 90° left-hand turn and orbits the human clockwise at a radius d_h . Once between human and goal, it turns left and proceeds directly towards the target. While not being user-demonstrations, the distinct pattern enables a clear performance analysis, as its behavior is by design contradictory

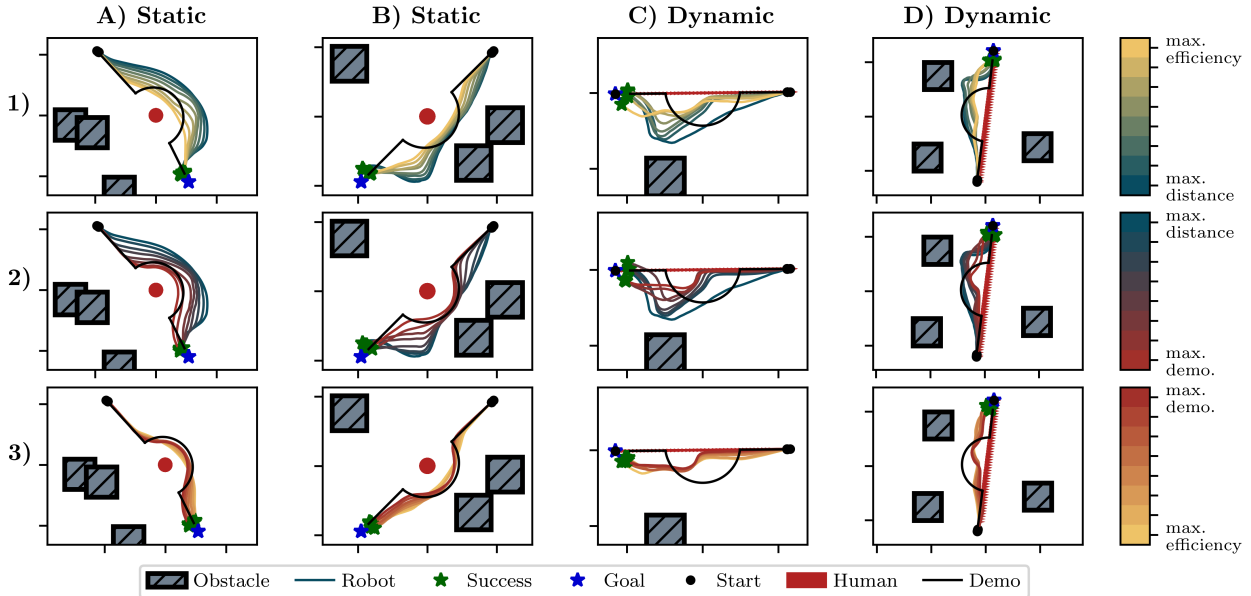


Fig. 3: Trajectory rollouts for different preference vectors (**rows**) and different scene setups of a static and a dynamic approaching human (**columns**). As can be seen, the navigation policy shifts its behavior according to the set preference. The colorbars on the right indicate the interpolated preference space Λ_i for each plot row. While shifting **Row 1**) from shortest driving behavior under the maximum efficiency preference (yellow) to distance-keeping (blue), the minimum distance to the human increases. At the same time, a tendency to navigate alongside obstacles - if present close to the path - has developed. Shifting towards the maximum demonstration preference (**Row 2**), the trajectory shapes increasingly resemble the demonstration pattern (black). On the shift back to maximum efficiency (**Row 3**), the demonstration pattern disappears in favor of shortest trajectories. Comparing the static (**A+B**) vs. dynamic human (**C+D**), the demonstration preference reflection loses shape as the agent struggles to follow the static pattern that moves with the now dynamic human, yet efficiency and distance preferences keep up with a moving human.

to the other two objectives, efficiency and distance-keeping. Specifically, the trajectories are only partially goal-directed, conflicting $r_{\text{efficiency}}^t$ and traverse close to the human at $d_h = 1\text{m}$, contradicting r_{distance}^t with an impact radius of 2m . Anchored solely around the human and goal position, we can easily augment the single demonstration trajectory by rolling it out N_D times in randomized obstacle configurations, recording only collision-free rollouts. The resulting dataset is handed to the D-REX pipeline, as elaborated in Sec. III-C. The final reward term is $r_{\text{demo}}^t = -10 \cdot (\hat{R}_\theta(s_t, a_t) - 1)$.

IV. EXPERIMENTAL EVALUATION

With our experimental evaluation, we aim to find proof for the following research claims:

- C1: The D-REX-based reward model successfully captures and teaches the demonstration patterns to the agent.
- C2: Our framework produces a preference-adaptable yet reliable navigation policy.
- C3: Our policy generalizes from simulation to the real world, even on a robot not used for training.

We will perform a qualitative analysis that discusses the behavior diversity on selected navigation scenarios, followed by a quantitative analysis averaging navigation task-relevant metrics over a larger number of trajectories. Our evaluation concludes with a sim-to-real transfer and evaluation on two robots.

A. Training and Environment

We train using the iGibson simulator [25] with a simulated Kobuki Turtlebot 2. Robot start and goal positions are randomly sampled, 6 to 12m apart in open space. A static

human is placed between them, aligning with a static-human demonstration pattern. Three static rectangular obstacles are randomly placed, avoiding occupied positions. The robot must navigate to the goal while avoiding both the human and obstacles, which may conflict with the human distance-keeping objective. Training is conducted for 600k steps across $C_p = 3$ environments, using $\gamma = 1.0$, and the final model is used for evaluation. For the evaluation of generalization to dynamic environments only, not training, we simulate a dynamic human approaching the robot with an opposite start goal configuration.

B. Qualitative Navigation Analysis

Figure 3 shows navigation strategies of our MORL agent in static (A+B) and dynamic human (C+D) scenarios, under varying preference weights and obstacle configurations. Three subplot rows interpolate convex preferences between pairwise combinations of two objectives, with the third objective fixed at zero. In Row 1, preferences interpolate between distance and efficiency, parameterized by $\mu \in [0, 1]$, with the vector $\lambda_1(\mu) = (0, \mu, 1 - \mu)$. The other rows follow similar pairwise combinations. The resulting set of $\lambda_i(\mu)$ is $\Lambda_i = \left\{ \left(\frac{i}{N}, 1 - \frac{i}{N}, 0 \right) \mid \mu = \frac{i}{N}, i = 0, \dots, N \right\}$ with $N = 10$, forming the test set $\Lambda = \Lambda_1 \cup \Lambda_2 \cup \Lambda_3$, see Sec. IV-C.

The plots depict the robot's trajectories from an initial point (black dot) to a goal (blue star), considering static obstacles and a human (red circle & arrow), with the oracle demonstration trajectory (black line) included.

Starting with the static human in Fig.3A+B, the shift from efficiency to distance-keeping (Fig.3.1) shows increasing human distance along the path, with the robot eventually

passing closely without collision, reducing path length due to the efficiency penalty $r_{\text{efficiency}}^t$. Under maximum human distance preference, the robot occasionally stays close to obstacles before turning towards the goal after passing them.

For the shift from distance-keeping to demonstration-like behavior (Fig. 3.2), the minimum distance to the human decreases. Supporting C1, trajectories shape into the characteristic demonstration pattern of straight approach, circular circumnavigation, and a goal-directed turn, yet sharp corners near the human are less pronounced than in the demonstration.

Finally, shifting preferences from demonstration back to efficiency (Fig. 3.3), demonstration-driven trajectories bend around the human, while efficiency-driven ones head directly to the goal after passing. When obstacles are near the human, collisions are avoided, though at reduced distance. Under maximum distance preference, human distance is maintained before and after obstacles, and all trajectories pass the human on the right, following the demonstration pattern.

In the dynamic setting not included during training, with a human approaching at 0.5 m s^{-1} (Fig. 3.C+D), the efficiency and distance-keeping objectives are maintained without collisions. The avoidance maneuvers occur more abruptly than in the static case, bending sharply away from the human. As expected, the demonstration pattern is less followed, with the orbiting part shrinking or not completed due to the moving human.

These results provide evidence for C1 and C2, showing the robot’s ability to adjust its behavior from human-distant to demonstration-driven and efficiency-focused navigation.

C. Quantitative Analysis

1) *Preference Reflection*: We conducted a quantitative evaluation of the preference-reflecting agent using multiple performance and navigation metrics (Fig. 4). The agent was tested across 100 episodes in random environments, using different interpolated preference weights $\lambda \in \Lambda$ (colored fractions in Fig. 4e; see Sec. IV-B). Statistical significance between mean values for the maximum preferences was assessed using a Student’s t-test.

The agent (OUR) achieved a success rate of 100% with no timeouts or collisions (Table I, first column). As the distance preference increases, both minimum human distance and navigation time rise (Fig. 4a+d), indicating longer trajectories to maintain greater human distance.

To assess how well the demonstration trajectory is reflected (claim C1), we computed the Fréchet distance between the demonstration and executed trajectories (Fig. 4b). The minimum Fréchet distance of 0.41m occurs when demonstration preference is maximized. Efficiency and distance-keeping preferences also reduce the Fréchet distance, as the demonstration path passes close to the human.

Comparing the trends of minimum lidar-recorded obstacle distance ($\min(d_{\text{obst}})$, Fig. 4c) and minimum human distance ($\min(d_h)$, Fig. 4d), the agent clearly distinguishes between humans and static obstacles. As the human distance preference increases, the robot maintains a larger distance from

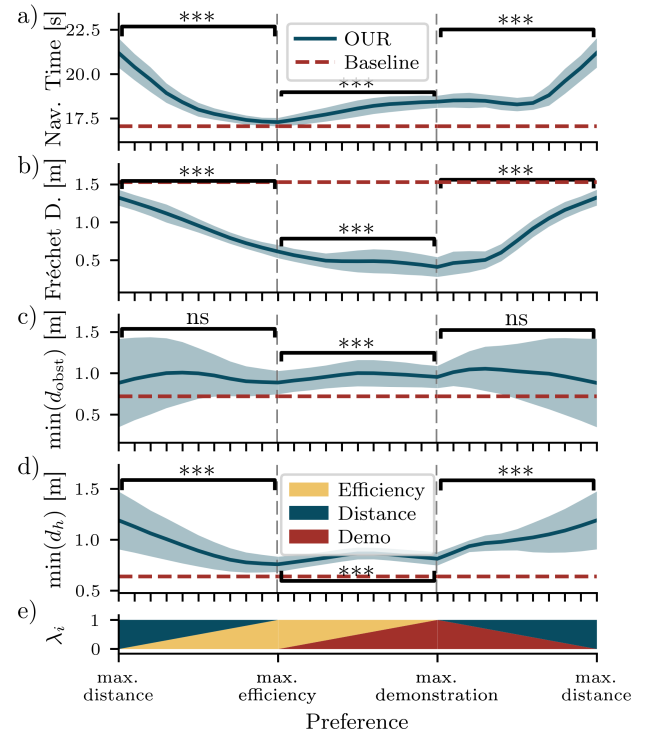


Fig. 4: Quantitative metrics of OUR agent for different preference configurations (e), tested for statistical significance for dissimilar mean between the maximum preferences, with *** for $p \leq 0.001$, and ns for no significance. **a**) The navigation time is smallest for maximized efficiency preference, as expected. **b**) The Fréchet distance to the demonstration trajectory decreases as the demonstration preference increases. **c**) The minimum distance to any obstacle is taken directly from the lidar sensor, revealing a differentiation between any obstacle and the human: **d**) The minimum distance to the human grows with its preference weight. A non-MORL baseline agent (red dotted line) that only obeys the baseline reward term of collision-avoidance and goal-pursuance is included in each plot.

the human, while staying close to obstacles, accepting higher collision risk to prioritize proxemic preferences.

This quantitative analysis supports the findings from the qualitative evaluation, providing measurable evidence for research claims C1 and C2.

2) *Baseline*: A non-MORL policy that only obeys the navigational baseline rewards r_{baseline} (goal and collision) was trained and quantitatively analyzed, compare the red dotted line in Fig. 4. Here, two metrics stand out: While the MORL agent trades human for obstacle distance, the baseline agent lacking the human-distance reward treats both the human and static obstacles similarly. For this reason, a similar minimum

Metric	λ	OUR	-NH	-RM	-RM-NH	$-\gamma$
SR↑ [%]	$\lambda_i \in \Lambda$	100	96.8	100	79.6	96.0
CR↓ [%]	$\lambda_i \in \Lambda$	0	2.7	0	11.4	4.0
TR↓ [%]	$\lambda_i \in \Lambda$	0	0.5	0	9.0	0.0
$\min(d_h) \uparrow$ [m]	λ_{dist}	1.18	0.52	1.16	0.48	1.22
Fréchet↓ [m]	λ_{demo}	0.41	0.57	0.46	0.49	0.50
Nav. time↓ [s]	λ_{eff}	17.3	16.9	17.4	19.2	18.3

TABLE I: Ablation study with respect to the state space and reward model, bold number highlighting the highest performance. For the ablation identifiers and preference vectors $\{\lambda_{\text{dist}}, \lambda_{\text{demo}}, \lambda_{\text{eff}}\}$, please refer to Sec. IV-C.3. For brevity, the identifiers are shortened after OUR, so that, e.g., -NH corresponds to OUR-NH with the human pose state excluded. The results were averaged over 100 trajectories for single λ , and for the success rate (SR), collision rate (CR), and timeout rate (TR) additionally over all $\lambda_i \in \Lambda$.

value for $d_h = 0.64\text{m}$ and $d_{\text{obst}} = 0.72\text{m}$ is measured for the baseline agent, in clear contrast to the MORL agent. Also, a higher demonstration Fréchet distance confirms the lack of demonstration knowledge.

3) *Ablation Study*: We ablated the architecture with respect to the state space and demonstration reward model, compare Table I. The state space changes apply to all involved models: D-REX BC policy, D-REX reward model, actor, and critic. The ablations cover exclusion of human position (OUR-NH), removal of the action as input to the reward model leaving $r_{\text{demo}}^t = \hat{R}_\theta(s_t)$ (OUR-RM), the combination of both (OUR-RM-NH), and a lower discount value of $\gamma = 0.99$ (OUR- γ). Note that the maximum preference vectors in Table I are $\lambda_{\text{demo}} = (1, 0, 0)$, $\lambda_{\text{dist}} = (0, 1, 0)$, $\lambda_{\text{eff}} = (0, 0, 1)$, respectively.

Compared to OUR, removing the human position from the state space in OUR-NH and OUR-RM-NH reduces distance-reflection capabilities. This is expected due to the correlation between human position and distance preferences in demonstrations, and it highlights the agents' inability to distinguish between humans and obstacles in low-resolution lidar. While OUR-RM offers similar collision-free performance, its preference-reflection is slightly weaker than OUR. OUR- γ shows better human distance-keeping but leads to more collisions and weaker adaptation to demonstration and efficiency. Experiments with lower γ (e.g., $\gamma = 0.95$) did not converge, likely due to the agent's tendency to defer goal rewards under higher γ to better align with preference objectives.

D. Real-World Transfer

We evaluated our tuneable policy on a Kobuki Turtlebot 2 using ROS [26] and transferred the Turtlebot-trained policy to a Toyota Human Support Robot (HSR). For localization, we used AMCL [27] with a pre-mapped environment from Gmapping [28]. The agent received ground truth human and goal positions, with the dynamic human localized via a Vive VR tracker. Due to the HSR's 270° lidar coverage, compared to the Turtlebot's 360°, we padded the rear values with the maximum range of 4m, assuming rear obstacles would not affect performance since the robot drives forward only. The HSR's lidar, mounted at the front of its rotation center, may cause state space discrepancies. We then ran navigation tests on both robots for the preference vectors λ in Λ with $N = 5$ (see Sec.IV-B).

The recorded Turtlebot trajectories are shown in Fig. 5.A and the HSR trajectories in Fig. 5.B, overlaid with the localization map. Both robots adapt their navigation according to preferences. For maximum distance (Fig. 5.A1), the Turtlebot shows oscillations due to slight over-steering, while the HSR drives closer to obstacles and exhibits wiggly motion near the goal (Fig. 5.B1), likely due to lidar state-mismatch from the padded rear values. For maximum demonstration reflection, the Turtlebot's trajectory aligns better with the demonstration than the HSR (Fig. 5.2).

Collision-free behavior is maintained among dynamically approaching humans (Fig. 5.C+D). As in the dynamic simulations experiments (Fig. 3), avoidance sharpens for the

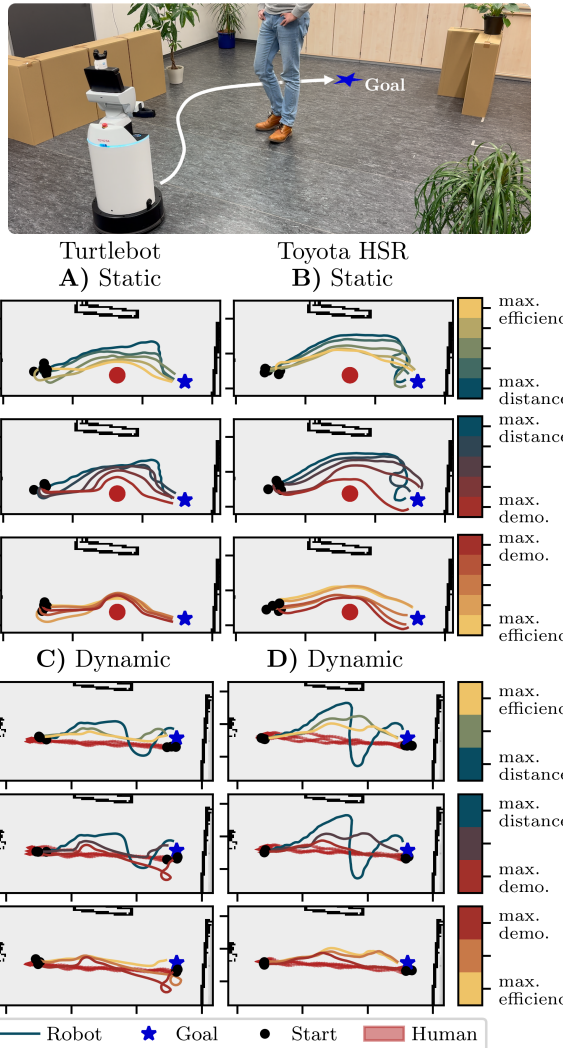


Fig. 5: Real-world experiment setup (**top**) and results (**bottom**) with the policy OUR in a (**left**) sim-to-real transfer with the Kobuki Turtlebot 2 and a (**right**) the Toyota HSR. With a static human as during training (**A+B**), the navigation behavior in real world successfully reflects varying the preferences on both robots. While the Turtlebot exhibits better demonstration reflection, the HSR keeps more distance to the human under the maximum distance preference. Among the dynamic approaching human (**C+D**) not accounted for during training, the preference-reflection decreases.

demonstration objective but fades as the human and robot pass each other. Overshooting behind the human for the distance preference may result from increased distance observations.

The real environment had more obstacles than the simulation, highlighting the system's sim-to-real generalization. See the supplemental video for real-world experiments. In conclusion, the policy transfers smoothly to real robots, supporting research claim C3.

V. CONCLUSION

In summary, we introduced an innovative framework fusing multi-objective reinforcement learning (MORL) with demonstration-based learning for adaptive, personalized robot navigation in human environments. Our approach successfully modulates the conflicting objectives of distance keeping, navigational efficiency, and the amount of demonstration reflection without retraining. To achieve this,

we distill demonstration data into a reward model that shapes the agent's trajectories during navigation with variable strength. In various qualitative and quantitative experiments, we demonstrated the adaption capability to varying preferences and scenarios. Finally, we successfully deployed the agent on two real robots.

While the amount of demonstration-reflection can be modulated, a limitation of our approach is the inability to alter the demonstration data itself without retraining, limiting the instant preference modulation to the defined preference space. This poses an interesting avenue for future research. We believe that designing robot policies in a multi-objective, tuneable manner is a step forward in developing robots capable of seamlessly integrating into human-centric spaces.

REFERENCES

- [1] P. Vamplew, R. Dazeley, C. Foale, S. Firmin, and J. Mummery, "Human-aligned artificial intelligence is a multiobjective problem," *Ethics and Information Technology*, vol. 20, no. 1, Mar. 2018.
- [2] J. de Heuvel, N. Corral, L. Bruckschen, and M. Bennewitz, "Learning Personalized Human-Aware Robot Navigation Using Virtual Reality Demonstrations from a User Study," in *2022 31th IEEE International Conference on Robot Human Interactive Communication (RO-MAN)*, 2022.
- [3] C. Mavrogiannis, F. Baldini, A. Wang, D. Zhao, P. Trautman, A. Steinfield, and J. Oh, "Core Challenges of Social Robot Navigation: A Survey," *ACM Transactions on Human-Robot Interaction*, vol. 12, Feb. 2023.
- [4] C. Pérez-D'Arpino, C. Liu, P. Goebel, R. Martín-Martín, and S. Savarese, "Robot Navigation in Constrained Pedestrian Environments using Reinforcement Learning," in *2021 IEEE International Conference on Robotics and Automation (ICRA)*, May 2021.
- [5] J. de Heuvel, N. Corral, B. Kreis, J. Conradi, A. Driemel, and M. Bennewitz, "Learning Depth Vision-Based Personalized Robot Navigation From Dynamic Demonstrations in Virtual Reality," in *2023 IEEE/RSJ International Conference on Intelligent Robots and Systems (IROS)*, Oct. 2023.
- [6] D. Marta, S. Holk, C. Pek, J. Tumova, and I. Leite, "Aligning Human Preferences with Baseline Objectives in Reinforcement Learning," in *2023 IEEE International Conference on Robotics and Automation (ICRA)*, May 2023.
- [7] C. F. Hayes, R. Rădulescu, E. Bargiacchi, J. Källström, M. Macfarlane, M. Reymond, T. Verstraeten, L. M. Zintgraf, R. Dazeley, F. Heintz, E. Howley, A. A. Irissappane, P. Mannion, A. Nowé, G. Ramos, M. Restelli, P. Vamplew, and D. M. Roijers, "A practical guide to multi-objective reinforcement learning and planning," *Autonomous Agents and Multi-Agent Systems*, vol. 36, no. 1, Apr. 2022.
- [8] J. Choi, C. Dance, J.-e. Kim, K.-s. Park, J. Han, J. Seo, and M. Kim, "Fast Adaptation of Deep Reinforcement Learning-Based Navigation Skills to Human Preference," in *2020 IEEE International Conference on Robotics and Automation (ICRA)*. IEEE, May 2020.
- [9] L. Keselman, K. Shih, M. Hebert, and A. Steinfield, "Optimizing Algorithms from Pairwise User Preferences," in *2023 IEEE/RSJ International Conference on Intelligent Robots and Systems (IROS)*, Oct. 2023.
- [10] G. Ferrer and A. Sanfeliu, "Anticipative kinodynamic planning: Multi-objective robot navigation in urban and dynamic environments," *Autonomous Robots*, vol. 43, no. 6, Aug. 2019.
- [11] S. Kumar and A. Sikander, "A modified probabilistic roadmap algorithm for efficient mobile robot path planning," *Engineering Optimization*, vol. 55, no. 9, Sept. 2023.
- [12] S. B. Banisetty, S. Forer, L. Yliniemi, M. Nicolescu, and D. Feil-Seifer, "Socially Aware Navigation: A Non-linear Multi-objective Optimization Approach," *ACM Trans. Interact. Intell. Syst.*, vol. 11, no. 2, July 2021.
- [13] R. Yang, X. Sun, and K. Narasimhan, "A Generalized Algorithm for Multi-Objective Reinforcement Learning and Policy Adaptation," in *Advances in Neural Information Processing Systems*, vol. 32. Curran Associates, Inc., 2019.
- [14] T. Basaklar, S. Gumussoy, and U. Y. Ogras, "PD-MORL: Preference-Driven Multi-Objective Reinforcement Learning Algorithm," *Proceedings of the 11th International Conference on Learning Representations*, 2023.
- [15] J. Xu, Y. Tian, P. Ma, D. Rus, S. Sueda, and W. Matusik, "Prediction-Guided Multi-Objective Reinforcement Learning for Continuous Robot Control," in *Proceedings of the 37th International Conference on Machine Learning*. PMLR, Nov. 2020.
- [16] F. Felten, L. N. Alegre, A. Nowé, A. Bazzan, E. G. Talbi, G. Danoy, and B. C. da Silva, "A Toolkit for Reliable Benchmarking and Research in Multi-Objective Reinforcement Learning," *Advances in Neural Information Processing Systems*, vol. 36, 2023.
- [17] X. He and C. Lv, "Toward personalized decision making for autonomous vehicles: A constrained multi-objective reinforcement learning technique," *Transportation Research Part C: Emerging Technologies*, vol. 156, Nov. 2023.
- [18] S. Huang, A. Abdolmaleki, G. Vezzani, P. Brakel, D. J. Mankowitz, M. Neunert, S. Bohez, Y. Tassa, N. Heess, M. Riedmiller, and R. Hadsell, "A Constrained Multi-Objective Reinforcement Learning Framework," in *Proceedings of the 5th Conference on Robot Learning*. PMLR, Jan. 2022.
- [19] G. Cheng, Y. Wang, L. Dong, W. Cai, and C. Sun, "Multi-objective deep reinforcement learning for crowd-aware robot navigation with dynamic human preference," *Neural Computing and Applications*, June 2023.
- [20] A. Ballou, X. Alameda-Pineda, and C. Reinke, "Variational meta reinforcement learning for social robotics," *Applied Intelligence*, vol. 53, no. 22, Nov. 2023.
- [21] K. Lee, S. Kim, and J. Choi, "Adaptive and Explainable Deployment of Navigation Skills via Hierarchical Deep Reinforcement Learning," May 2023.
- [22] M. Andrychowicz, F. Wolski, A. Ray, J. Schneider, R. Fong, P. Welinder, B. McGrew, J. Tobin, O. Pieter Abbeel, and W. Zaremba, "Hindsight Experience Replay," in *Advances in Neural Information Processing Systems*, vol. 30. Curran Associates, Inc., 2017.
- [23] D. S. Brown, W. Goo, and S. Niekum, "Better-than-Demonstrator Imitation Learning via Automatically-Ranked Demonstrations," in *Proceedings of the Conference on Robot Learning*. PMLR, May 2020.
- [24] R. A. Bradley and M. E. Terry, "Rank analysis of incomplete block designs: I. The method of paired comparisons," *Biometrika*, vol. 39, no. 3/4, 1952.
- [25] C. Li, F. Xia, R. Martín-Martín, M. Lingelbach, S. Srivastava, B. Shen, K. Vainio, C. Gokmen, G. Dharan, T. Jain, A. Kurenkov, C. K. Liu, H. Gweon, J. Wu, L. Fei-Fei, and S. Savarese, "iGibson 2.0: Object-Centric Simulation for Robot Learning of Everyday Household Tasks," *arXiv:2108.03272 [cs]*, Nov. 2021.
- [26] M. Quigley, K. Conley, B. Gerkey, J. Faust, T. Foote, J. Leibs, R. Wheeler, and A. Y. Ng, "ROS: An open-source Robot Operating System," in *ICRA Workshop on Open Source Software*, vol. 3. Kobe, Japan, 2009.
- [27] D. Fox, W. Burgard, F. Dellaert, and S. Thrun, "Monte carlo localization: Efficient position estimation for mobile robots," *Aaaai/iaai*, vol. 1999, no. 343-349, 1999.
- [28] G. Grisetti, C. Stachniss, and W. Burgard, "Improving Grid-based SLAM with Rao-Blackwellized Particle Filters by Adaptive Proposals and Selective Resampling," in *Proceedings of the 2005 IEEE International Conference on Robotics and Automation*. IEEE, 2005.